# Mathematical modelling and gas sensing abilities of graphene based optical sensor

A. DENIZ[1], S.C. ACIKBAS[1], K. BUYUKKABASAKAL[2], Y. ACIKBAS[3,*], M. ERDOGAN[4], R. CAPAN[4]
*[1]Department of Mathematics, Faculty of Science, University of Usak, Turkey*
*[2]Department of Electric-Electronic Engineering, Faculty of Engineering, University of Usak, Turkey*
*[3]Department of Material Science and Nanotechnology Engineering, Faculty of Engineering, University of Usak, Turkey*
*[4]Department of Physics, Faculty of Science, University of Balikesir, Turkey*

In this work, graphene based Langmuir-Blodgett (LB) thin films prepared onto gold-coated glass substrates to evaluate its sensing ability by using Surface Plasmon Resonance (SPR) system. In order to illuminate the swelling characteristics of the graphene optical sensor, the diffusion coefficients of these vapors were calculated by applying the early-time Fick's diffusion equation. The diffusion coefficients are found to be $0.1954 \times 10^{-15}$, $0.0696 \times 10^{-15}$ and $0.0197 \times 10^{-15}$ cm$^2$ s$^{-1}$ for benzene, toluene, and xylene, respectively. The nonlinear autoregressive with exogenous input neural network was designed by utilizing experimental data from SPR kinetic results to model the change in photodetector response. The calculated diffusion coefficients using artificial neural network model are approximately equal to real-data diffusion coefficients as verified by very high correlation coefficients ($0.1948 \times 10^{-15}$, $0.0760 \times 10^{-15}$ and $0.0198 \times 10^{-15}$ cm$^2$ s$^{-1}$ for benzene, toluene, and xylene, respectively). Consequently, graphene-based optical sensors displays high response and sensitivity for saturated benzene vapor than other vapors. These optical thin film sensors were potential candidates for organic vapor sensing applications with simple and low cost preparation at room temperature.

## 1. Introduction

With the rapid advancement in industrial area, the environment health has been affected and these developments have led to an increase in air pollution. This pollution has severely affected the day-to-day life of people that includes harmful volatile organic compounds (VOCs), dusts and toxic smokes. Among them, VOCs are the most hazardous materials, which threaten the earth we live today. Therefore, the detection of VOCs play crucial role in different fields such as air quality monitoring [1], industrial safety [2] and medical diagnosis [3]. Interest in the detection of VOCs at high sensitivity and low detection limit has risen over the past decade.

In recent years, there is an increasing demand for improvement of the sensing materials, which can detect VOCs, including nanocomposites [4], macromolecules [5], polymers [6], ionic liquids [7] and carbon-based materials [8] with low detection limits. Among the available materials, graphene, graphene oxide (GO) and reduced graphene oxide (rGO) as carbon-based materials have already been used as a chemical sensor because these material shows excellent properties, such as a heat conductivity, high-speed electron mobility at room temperature, a large number of chemically active sites, specific surface area and unique hydrophilic properties [9,10]. A suitable kinetic measurement technique to the detection of VOCs is as important as choose of the sensitive materials in chemical sensor applications. Surface Plasmon

Resonance (SPR) is one of the most preferred techniques to investigate the interaction between two molecules (host-guest molecules) of interest due to its significant advantages such as high reliability and real-time analysis with high sensitivity [11].

Developing mathematical model of an experimental process helps to analyze the experimental study with an analytical approach. Among these mathematical models, artificial neural networks are one of useful tools for modeling nonlinear data and processes [8]. Artificial neural networks are widely used in data modeling due to its less complexity, inclusion of low-cost calculations and learning capacity [12]. Artificial neural networks have become popular research topic due to its interdisciplinary features. Independent from the area of application, it can be used for modelling any data. Considering the literature, many studies in different science areas for data modelling using ANNs can be found such as the modelling of: the physiological processes [13], the capacities of carbon dioxide absorption for some materials [14], the gyroscope platform [15], nonlinear responses of the radio frequency (RF) amplifier [16], the load displacements curves [17], and the magneto-rheological damper [18]. In another studies, the mathematical models are developed to solve the cutting force problem for metals [19] and for railway electrical consumption using ANN model [20].

This work focuses on investigation of VOCs swelling behaviors of graphene-based LB thin film molecule using early-time analysis of Fick's law of diffusion based on the

change in the reflected light intensity. The graphene-based SPR optical sensor films are subjected to the saturated aromatic BTX (benzene, toluene, xylene) hydrocarbons for investigating the swelling mechanism in the sensor application. To the best of our knowledge, this is the first report on graphene swelling properties and an accurate calculation of diffusion coefficients of selected VOCs for graphene-based LB thin films, which are tested with SPR technique. Thanks to the designed NARX-ANN model, the calculated diffusion coefficients from Fick's diffusion equation can be validated.

mL$^{-1}$ concentration of graphene and chloroform + DMF solutions was prepared to use during the fabrication of graphene LB thin film onto gold-coated glass substrates. The Y type (the selected deposition type) graphene LB thin films were prepared at a surface pressure of 18 mN m$^{-1}$, and this suitable value was determined from the isotherm graph which was reported in our previous study [21]. All graphene LB thin film fabrication process was fixed at room temperature.

## 2. Experimental details

### 2.1. Preparation of graphene LB thin film

Fig. 1 presents the chemical structure of graphene molecule which is selected LB thin film materials. 1.88 mg
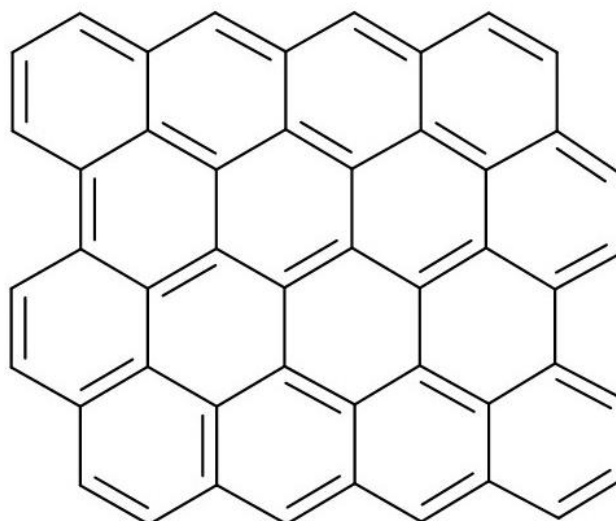


*Fig. 1. Chemical structure of graphene molecule*

### 2.2. SPR measurement technique

The SPR technique is based on the principle that incident light can stimulate free electrons delocalized on a metallic film to generate surface plasmons under particular conditions. The SPR technique, which is one of the main optical techniques, can measure host-guest interactions in real time and allows monitoring of poorly bound interactions due to its high degree of surface sensitivity. A binding contact between the surface and the target molecules changes the local refractive index, causing the SPR angle to shift. To obtain selectivity for specific chemicals or biomolecules, the sensor surface is functionalized with selective receptors. The SPR technique is being utilized to develop low-cost, high-resolution chemical and biochemical optical sensors. Since

the metal film, incident light and temperature are constant in experiments, SPR signals obtained in the kinetic measurements are directly dependent on the shift in refractive index of the sensor surface environment. In this study, a BIOSUPLAR 6Model SPR Spectrometer was utilized to perform all SPR kinetic measurements. During the SPR measurements: (i) a glass prism (with a refractive index of 1.515) was fixed to a holder to take measurements in an air environment, (ii) a laser diode at a wavelength of 632.8 nm was employed as a light source, and (iii) gold-coated (50 nm) glass slides were used to obtain SPR signals. In all SPR kinetic experiments, the samples were exposed to VOCs for two minutes at a time, and then the recovery process was realized by injecting fresh air for another two minutes. Fig. 2 shows a symbolic representation of the SPR kinetic measurement system.
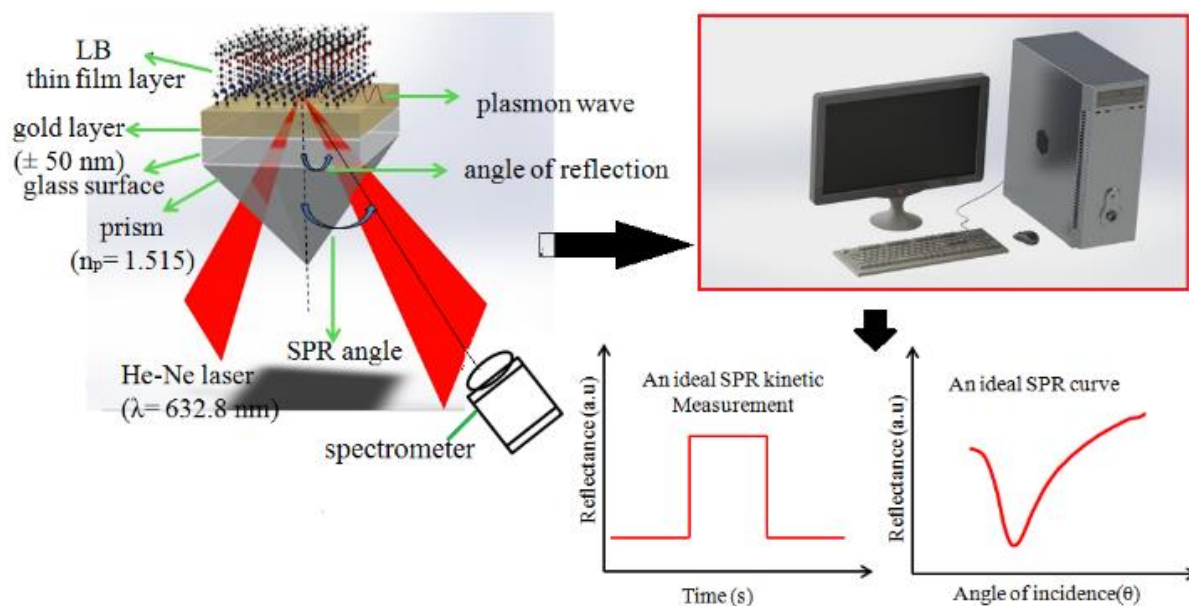
*Fig. 2. A shematic diagram of the surface plasmon resonance measurement system (color online)*

## 2.3. Neural network model

Artificial neural networks are widely used in nonlinear data modeling. ANNs are consist of input layer, hidden layer(s) and output layer. Each layer includes some amount of neurons which is determined by the user/programmer. Input layer accepts the input signals and using weights of neurons; transfers the weighted inputs to the hidden layer(s). Hidden layer(s) perform nonlinear transformations to its input signals. Output layer, by using the inputs from hidden layer, calculates the model output for ANN. Basic diagram of an artificial neural network is given in Fig. 3.
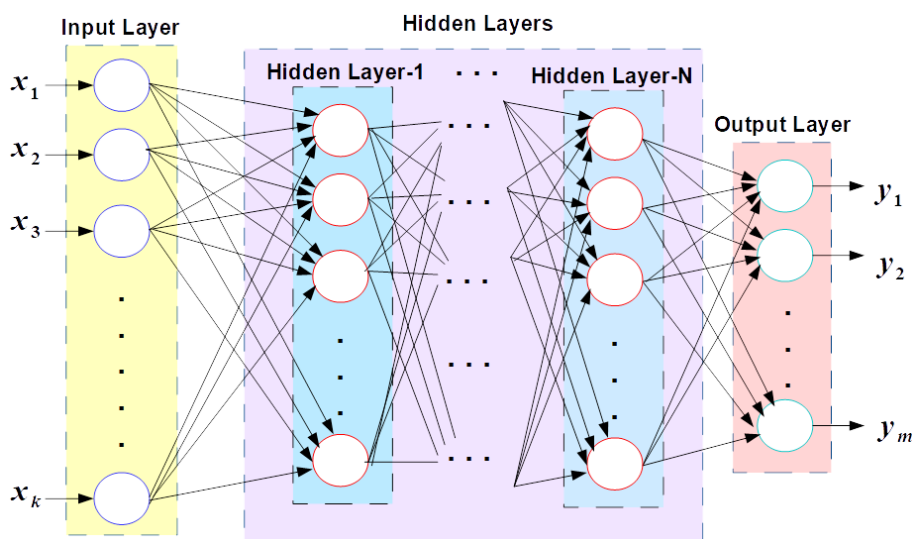


*Fig. 3. Basic diagram of an artificial neural network (color online)*

ANNs have different topologies to create a model using measurements. For this study, due to its success in nonlinear time series data modeling, a NARX-ANN is designed for setting up a model for the shifts in the reflected light intensity of benzene, toluene and xylene. NARX-ANNs are defined as artificial neural network with exogenous input. This type of ANN may use the time-shifted signals of both input and ANN output. Resulting output expression of ANN is a function of exogenous input and its output with delay(s).

For modeling the shifts in the reflected light intensity of benzene, toluene and xylene, a NARX-ANN given in Fig. 4 is designed. Designed NARX-ANN is consist of input layer, one hidden layer with 8 neurons and output layer.
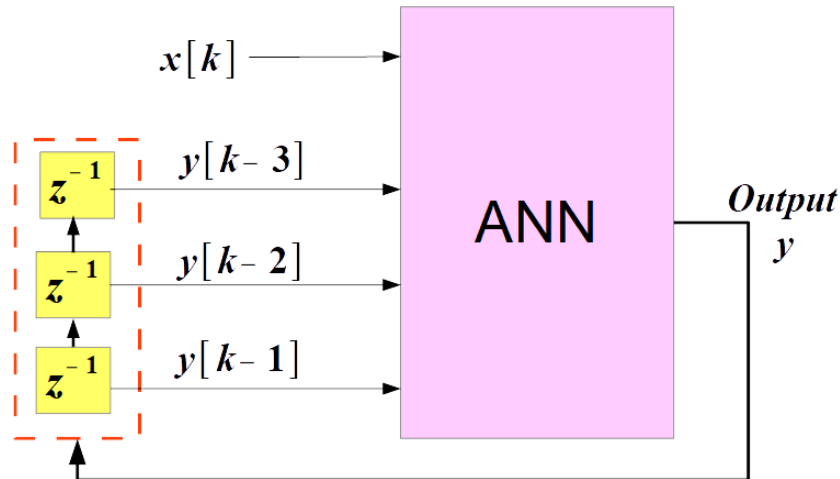
*Fig. 4. Architecture of designed NARX-ANN (color online)*

Input $x$ of the NARX-ANN is current value of time instant where $y[k-1]$, $y[k-2]$, $y[k-3]$ are time delayed samples of ANN model output and used as internal inputs to the ANN.

## 3. Result and discussion

### 3.1. Sensing properties of graphene-based optical sensor

In this work, kinetic measurements for a candidate chemical sensor material (*graphene*) sensitive to optical changes were carried out using SPR technique. In Fig. 5, a host-guest interaction between the graphene-based optical sensor and VOCs is presented by recording the photodetector responses as a function of time. Benzene,

toluene and xylene (BTX) were periodically released into the VOCs cell for 120 seconds, in the following order: fresh air-VOCs- fresh air-VOCs -…-fresh air. The responses of the graphene-based LB thin film to all BTX vapors increased abruptly due to the guest molecule's adsorption on the thin film, and then decreased exponentially over several seconds due to the initiation of the diffusion process. Then, the kinetic response of graphene-based optical sensor reaches the fixed value and it can be explained that the amount of the adsorbed and the desorbed molecules is approximately equal. At 240 s, the fresh air is moved to the surface of graphene-based optical sensor to observe whether the response value of optical sensor returns to the initial value or not.
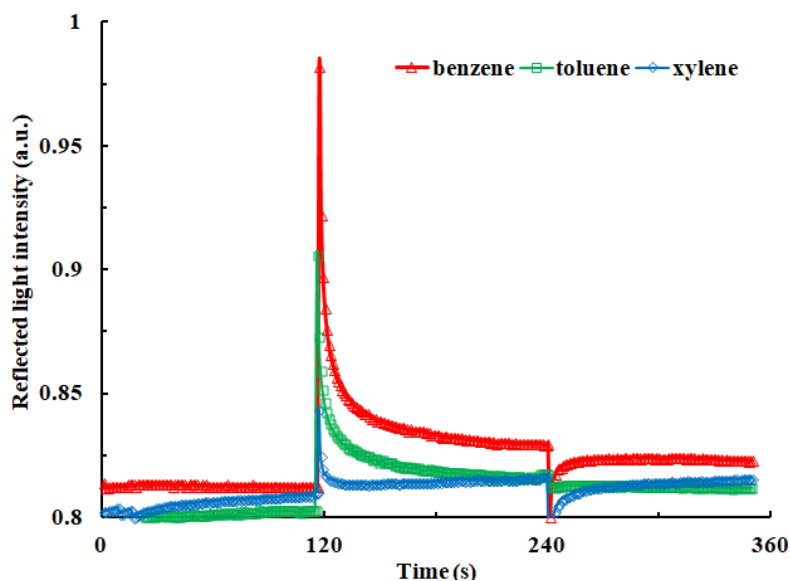


*Fig. 5. The photodetector responses of the graphene-based optical sensor (color online)*

The swelling dynamics of the graphene-based optical sensor were revealed by using Fick's second diffusion law [22] to calculate the diffusion coefficient values for all VOCs utilized in this work at saturated concentration. The diffusion process, which begins with the introduction of the vapor into the gas chamber, is responsible for the exponential decrease in sensor response, which is depicted in Fig. 5 in terms of reflected light intensity and occurs between 120 and 240 seconds.

Fig. 6 depicts a swelling cycle for three different VOCs, with the normalized intensity of reflected light plotted against the diffusion time, which begins at t= 0. The diffusion coefficients (D) of VOCs, as reported in our previous studies [11, 23], can be calculated using this data in the advanced early-time Fick's diffusion equation.
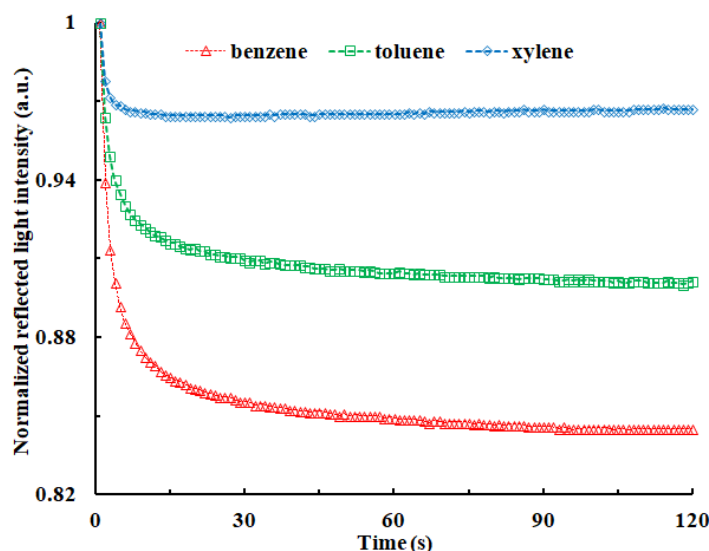


*Fig. 6. Normalized the photodetector response against swelling time for VOCs (color online)*

The normalized intensity of reflected light is plotted against the square root of swelling time in Fig. 7 (for benzene, toluene and xylene). The diffusion coefficient for the swelling of the graphene film can be calculated using the slopes of the linear regions. The diffusion coefficients for all VOCs are presented in Table 1.
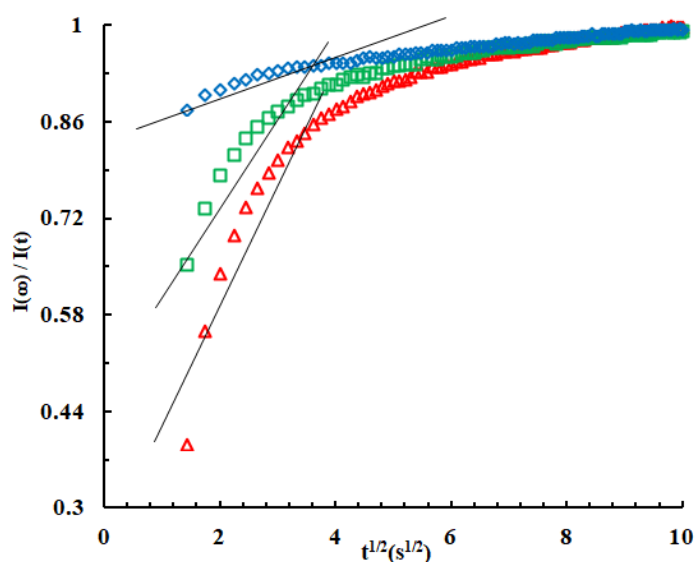


*Fig. 7. The square root of diffusion time versus the change in the intensity of reflected light graph for benzene (color online)*

All kinetic studies conducted with graphene-based optical SPR sensors demonstrate that the sensing response for the examined organic vapors is as follows: xylene < toluene < benzene. The values of diffusion coefficients for the graphene-based LB film sensors exhibit similar ordering

with the responses (the change in the intensity of reflected light) of the same film agains to organic vapors (*seen Table 1*). As reported in previous studies [24-26], this can be explained by differences in organic vapors' physical

properties, such as vapor pressure (at 20 °C) and molar volume.

Since benzene molecules have the highest value of vapor pressure (9.95 kPa) with its the lowest value of molar volume (86.36 cm$^3$ mol$^{-1}$) when it is compared with other vapors, they introduce into the graphene-based chemical sensor film is easier and faster. The responses of this optical chemical sensor in terms of the change in photodetector response for toluene (2.91 kPa; 107.10 cm$^3$ mol$^{-1}$) and m-xylene (0.80 kPa; 122.00 cm$^3$ mol$^{-1}$) are lower than benzene vapor because of these physical properties. It can be clarified with the vapor pressures of these VOCs, and it is well known that the higher vapor pressure leads to the bigger kinetic response [24]. In the light of these gas kinetic results, the other VOCs have higher values of molar volume can hardly diffuse into the graphene-based thin film in case they are compared with the diffusion of benzene vapor into the same thin film.

### 3.2. NARX-ANN modeling results

Performance and accuracy of NARX-ANN model is tested using real-time experimental measurements. NARX-ANN is trained using randomly selected 70% of the experimental data and 15% of the data is used for validation. NARX-ANN is tested using remaining 15% of the data. Then, NARX-ANN model results are compared with experimental data and accuracy of the proposed ANN model output is analyzed using statistical calculations such as correlation coefficient, mean-squared error and standard deviation.

Convergence of ANN model output to experimental data can be analyzed using Pearson's correlation coefficient as follows:

$$\rho(y, \hat{y}) = \frac{1}{N-1} \sum_{i=1}^{N} \left( \frac{y_i - \mu_y}{\sigma_y} \right) \left( \frac{\hat{y}_i - \mu_{\hat{y}}}{\sigma_{\hat{y}}} \right)$$

where $y$, $\hat{y}$ are the experimental and NARX-ANN model outputs, respectively; $\mu_y$ and $\mu_{\hat{y}}$ are the mean values for measurement and ANN model output, $N$ correspond to the number of measurements;, and $\sigma_y$, $\sigma_{\hat{y}}$ are standard deviation values of experimental data and ANN model output, respectively. $\rho(y, \hat{y})$ values close to "1" shows better fitting of model with experimental data.

ANN modeling results for benzene is given in Fig. 8. Considering both ANN model output and experimental data, modeling error for benzene is satisfactorily small which also can be seen from correlation coefficient between ANN model output and experimental data. Correlation coefficient is calculated as 0.99979 which shows the good convergence of the ANN model data to experimental data.
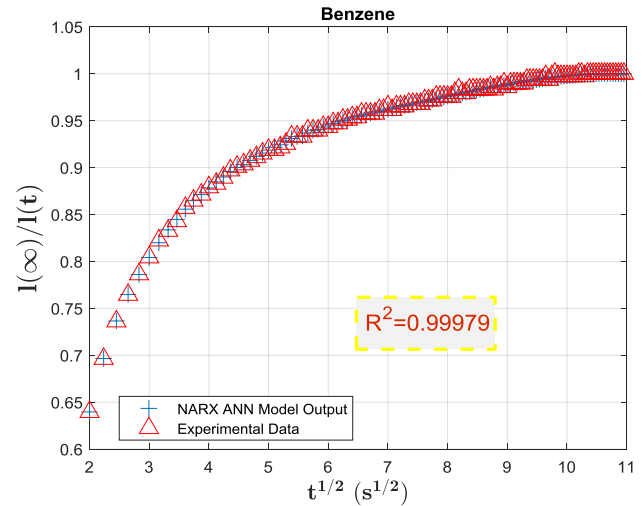


*Fig. 8. ANN modeling results of benzene (color online)*

Fig. 9 represents the NARX-ANN model results and experimental measurements of toluene. As seen from the plots, designed ANN model output approximately overlaps with real measurements. Correlation coefficient for toluene is calculated as "0.99883" which is nearly equal to "1" as desired.
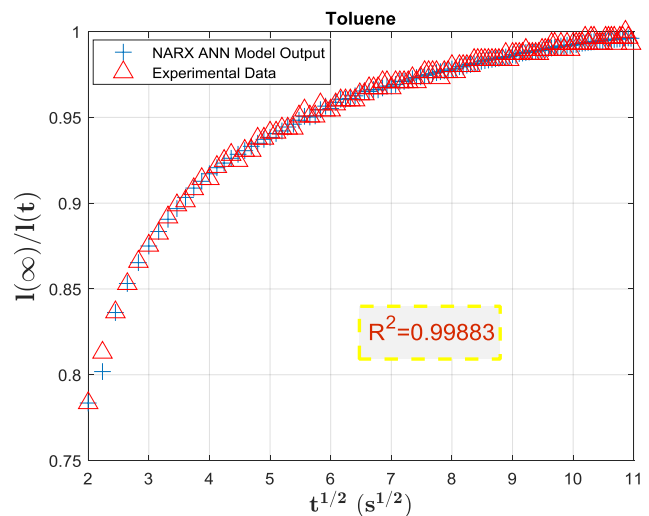


*Fig. 9. ANN modeling results of toluene (color online)*

Experimental data and NARX-ANN modeling results of xylene is given in Fig. 10. From Fig. 10, it is observed that correlation coefficient is 0.997 and modelling error for xylene is sufficiently small.
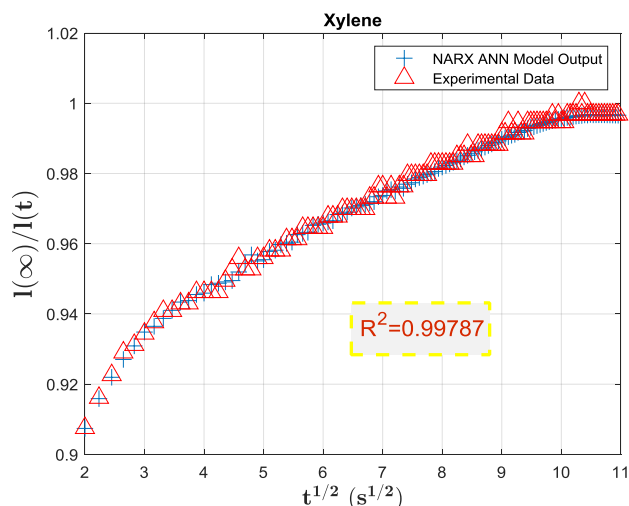
*Fig. 10. ANN modeling results of xylene (color online)*

Diffusion coefficients of both NARX-ANN model data and experimental data for benzene, toluene and xylene are calculated to compare the consistency of the ANN model output with real time data. Diffusion coefficient calculation result of these materials are given in Table 1.

*Table 1. Diffusion coefficients of ANN model and experimental data*

| Organic vapors | The experimental value of $D$ (cm$^2$ s$^{-1}$) × 10$^{-15}$ | The NARX value of D (cm$^2$ s$^{-1}$) × 10$^{-15}$ |
|---|---|---|
| Benzene | 0.1954 | 0.1948 |
| Toluene | 0.0696 | 0.0760 |
| Xylene | 0.0197 | 0.0198 |

Considering the diffusion coefficients of ANN model for these three organic vapors; diffusion coefficient values of ANN model are approximately equal to experimental data coefficients which exhibit the accuracy of the ANN model.

Table 2 gives the mean-squared error and standard deviations for NARX-ANN modelling error as performance metrics. Table-2 shows that, mean-squared error and standard deviations for benzene, toluene and xylene are satisfactorily small.

*Table 2. ANN modeling error performance metrics*

| Organic vapors | MSE(x10$^{-6}$) | Std. Dev. |
|---|---|---|
| Benzene | 1.7763 | 0.0013 |
| Toluene | 3.8137 | 0.0020 |
| Xylene | 2.0844 | 0.0014 |

## 4. Conclusion

The VOCs sensing abilities graphene-based optical sensor against trace vapor of aromatic BTX hydrocarbons were recorded in terms of the change in photodetector response or frequency of this sensor. Kinetic responses' values for these VOCs were ordered as xylene < toluene <

benzene, which was explained on the differences in the physical properties of VOCs. The swelling dynamic of the graphene optical sensor was illuminated with the development of the Fick's diffusion equation to calculate the diffusion coefficients of aromatic BTX hydrocarbons. Moreover, the diffusion coefficients of values were also calculated by utilizing the designed NARX-ANN model to support the diffusion coefficients which were calculated with the Fick's diffusion equation. The values of diffusion coefficients calculated with two different theoretical approaches verify that NARX-ANN fits experimental data with sufficiently small modelling errors.

Hereby, graphene material can be developed as a sensing material and may find potential applications in the development of room temperature optical sensing devices.

## References

[1] M. F. Yassin, A. M. Pillai, Int. J. Environ. Sci. Technol. **16**, 2733 (2019).
[2] S. Öztürk, A. Kösemen, Z. Şen, N. Kilinç, M. Harbeck, Sensors **16**(4), 423 (2016).
[3] A. D. Wilson, Sensors **18**(8), 2613 (2018).
[4] W. Chen, F. Deng, M. Xu, J. Wang, Z. Wei, Y. Wang, Sens. Act. B: Chem. **273**, 498 (2018).
[5] E. Ahmetali, H. P. Karaoğlu, Y. Urfa, A. Altındal, M. B. Koçak, Mater. Chem. Phys. **254**, 123477 (2020).
[6] Y. Chen, L. Wang, J. Kong, B. Shen, J. Xu, Chinese Chem. Lett. **31,** 2125 (2020).
[7] A. Rehman, X. Zeng, RSC Advances **5**, 58371 (2015)
[8] K. Büyükkabasakal, S. C. Acikbas, A. Deniz, Y. Acikbas, R. Capan, M. Erdogan, IEEE Sens. J. **19**, 9097 (2019).
[9] X. Li, Y. Chen, Z. Cheng, L. Jia, S. Mo, Z. Liu, Appl. Energy **130**, 824 (2014).
[10] T. A. Saleh, G. Fadillah, O. A. Saputra, TrAC Trends Anal. Chem. **118**, 194 (2019).
[11] E. Halay, S. Bozkurt, R. Capan, M. Erdogan, R. Unal, Y. Acikbas, Res. Chem. Intermed. **46(10)**, 4433 (2020).
[12] K. S. Narendra and K. Parthasarathy, IEEE Trans. Neural Netw. **1**(1), 4 (1990).
[13] M. B. Hossain, J. Moon, K. H. Chon, IEEE Access **8**, 186813 (2020).
[14] D. Bastani, M. E. Hamzehie, F. Davardoost, S. Mazinani, A. Poorbashiri, Fluid Phase Equilib. **354,** 6 (2013).
[15] Cheng, J. Xu, M. Wu, F. Li and S. Guo, 10th International Symposium on Computational Intelligence and Design (ISCID), Hangzhou, pp. 284-288 (2017).
[16] L. M. Aguilar-Lobo, J. R. Loo-Yau, S. Ortega-Cisneros, P. Moreno, J. A. Reynoso-Hernández, 2015 IEEE MTTS International Microwave Symposium, Phoenix, AZ, pp. 1-4 (2015).
[17] H. Rahmanpanah, S. Mouloodi, C. Burvill, S. Gohari, Helen M.S. Davies, Int. J. Eng. Sci. **154**,

103319 (2020).

[18] J. Fu, H. Yao, M. Yu, Y. Peng, Proceedings of the 32nd Chinese Control Conference, Xi'an, pp. 8769-8774 (2013)

[19] T. Szecsi, Journal of Materials Processing Technology **92–93**, 344 (1999).

[20] A. A. Komyakov, M. M. Nikiforov, V. V. Erbes, V. T. Cheremisin, V. I. Ivanchenko, 2016 IEEE 16th International Conference on Environment and Electrical Engineering (EEEIC), pp. 1-4 (2016).

[21] Y. Acikbas, J. Optoelectron. Adv. M. **18**(3-4), 220 (2016).

[22] J. Crank, The Mathematics of Diffusion: Oxford University, New York **19752**, 1 (1975).

[23] M. Erdogan, Y. Acikbas, C. Soykan, N. Cankaya, R. Capan, J. Optoelectron. Adv. M. **20**(9-10), 520 (2018).

[24] A. N. Kursunlu, Y. Acikbas, M. Ozmen, M. Erdogan, R. Capan, Colloids Surf. A Physicochem. Eng. Asp. **565**, 108 (2019).

[25] Y. Acikbas, G. Dogan, M. Erdoğan, R. Çapan, C. Soykan, Journal of Macromolecular Science, Part A **53**(8), 470 (2016).

[26] M. Ozmen, A.N. Kursunlu, Y. Acikbas, M. Erdogan, R. Capan, Applied Physics A **126**(3), 1 (2020).

_____

*Corresponding author: yaser.acikbas@usak.edu.tr